Retrieval and Use of High-Resolution Moisture and Stability Fields from Nimbus 6 HIRS Radiances in Pre-Convective Situations

DONALD W. HILLGER AND THOMAS H. VONDER HAAR

Department of Atmospheric Science, Colorado State University, Fort Collins 80523

(Manuscript received 22 October 1979, in final form 23 February 1981)

ABSTRACT

This is a study of environmental conditions prior to convective development on the Great Plains of the United States on four case study days in August 1975. The tool used was the High-resolution Infrared Radiation Sounder (HIRS) on Nimbus 6. A moisture-temperature retrieval scheme was developed to retrieve various lower tropospheric analysis and forecasting parameters from the HIRS radiances. Specifically, dew points and temperatures and other secondary parameters such as total precipitable water and static stability indices were derived and analyzed at a horizontal resolution of up to 30 km on these days. For the moisture parameters the comparisons to time-interpolated NWS rawinsonde values were especially good in spite of time and resolution differences. Comparisons with higher resolution synoptic surface observations of dew point and temperature were also good. The true quality of the mesoscale analyses, however, is only seen by examining the individual case study days. Small features at a scale of ~100 km, below the resolution of upper air and surface observations, were detected by the high-resolution satellite data. For example, perturbations on the dry line usually seen at this time of the year were apparent in the satellite data, although only the general dry line position was picked up by synoptic surface observations. The time lead also was important. Convective development starting from 2–2.5 h after the satellite pass at local noon did correlate well with the local maxima of moisture and instability seen in the satellite-derived analyses. A statistical structure analysis of the satellite-derived parameters also gave the highest signal-to-noise values for the moisture and stability parameters, whereas the temperature parameters showed much less signal-to-noise content. Results from these case study days, therefore, show the quality of high-resolution satellite-derived parameters and the applicability of this method of retrieving and using satellite soundings at the mesoscale.

1. Introduction and purpose

The determination of the quantitative structure of the moisture and temperature environment necessary for severe storm development is a desirable goal. A moist atmosphere is necessary for the release of latent heat through condensation. Moist areas of latent energy and the associated overlying or adjacent dry regions are known to be environmental severe storm indicators. In a similar manner, atmospheric masses of high thermal instability are primed for the release of potential energy. In many cases these various indicators of the severe or convective storm environment are only qualitatively known. Quantitative information about *mesoscale* (25 → 250 km) weather is limited except for some experimental monitoring associated with programs such as the Severe Environmental Storms and Mesoscale Experiment (Project SESAME, 1976; Lilly, 1975, 1977).

The first goal of the SESAME project relates directly to determination of such environmental parameters as mentioned above and their relation to the intensity of severe storm development. A second goal is to test the ability of new remote sensing systems as applied to such mesoscale problems. The satellite data used in this study are the product of one such remote sensing system which has seen improvements in channel selection and resolution in the last several years. Supposed failures of using satellite soundings in some cases (Traction and McPherson, 1977) may be due to its improper use (Kelly *et al.*, 1978). The retrieval and use of high-resolution moisture and temperature fields for mesoscale applications may be a proper application for satellite soundings since the satellite sounder inherently provides better horizontal resolution and coverage than its counterpart the rawinsonde (RAOB). Therefore, it is reasonable to use the satellite data in such a high-resolution mode to test its true ability as an instrument to provide mesoscale weather parameters.

The basis behind this study was to focus on preconvective environmental conditions. Satellite data obtained from the Vertical Temperature Profile Radiometer (VTPR), an early 1970's instrument, was used by the authors in a case study analysis

0027-0644/81/081788-19$08.75

of 24 April 1975 (Hillger and Vonder Haar, 1977) and in a statistical analysis of several NSSL (National Severe Storms Laboratory) sounding days in 1976 (Hillger and Vonder Haar, 1979). The results of this earlier work and that of others proved some lack of ability to determine lower tropospheric (especially moisture) parameters from satellite data. The problem resided in the inability to determine both temperatures and moisture from a sounder based on a single set of CO_2 spectral channels (only one H_2O and one window channel in the VTPR). A significant improvement in satellite instruments occurred in the late 1970's with the introduction of the Nimbus 6 High-resolution Infrared Radiation Sounder, HIRS (Smith *et al.*, 1975), with two water vapor channels and two infrared window channels. The radiances in these spectral regions are predominant in the moisture determination process. The HIRS instrument, therefore, has the capability of determining both moisture and temperature parameters from separate but not completely independent spectral regions.

Besides determining analysis and forecasting parameters, their distribution in space must be known. Storms usually develop along lines which are perpendicular to gradients in moisture, such as the dry line. From conventional data sources of less horizontal resolution these lines for potential development may appear to be rather uniform, but smaller scale variations along the lines are observed at higher resolution. An objective of this study was to examine the potential for determining and using these small-scale variations or perturbations seen in the satellite soundings. The satellite data will, therefore, be applied at the mesoscale where its advantage of high horizontal resolution may be realized.

It must be remembered that working with real radiances as opposed to simulated radiances at high resolution serves a need in that few studies have been done at that scale (Smith *et al.*, 1978, 1979; Wark *et al.*, 1974). These high-resolution soundings also provide a basis for a statistical analysis of the resulting satellite-derived parameters. Individual parameters were rated by a signal-to-noise ratio for the fields produced for the various case study days. A similar analysis have previously been accomplished for the VTPR instrument (Hillger and Vonder Haar, 1979). Those results showed that the satellite sounder is at least capable of detecting the same temperature gradient information as mesoscale rawinsonde soundings. However, the VTPR instrument was found inadequate for mesoscale moisture determination compared to special mesoscale RAOB networks. The results given here show a definite improvement in mesoscale moisture determination from HIRS-type satellite sounding radiances.

2. HIRS Moisture-temperature retrievals

Basically, there were three parameters which we wished to determine from the satellite-sensed radiances. The surface temperature, the moisture profile or the integrated moisture, and the temperature profile are all major influences on the radiances. The determination of these parameters required radiances from a window channel which is fairly free of molecular absorption, an H_2O absorption band, and a molecular absorption band of constant mixing ratio such as a CO_2 band. These three requirements were met by the HIRS instrument with two window channels at 3.7 and 11 μm, two H_2O channels at 6.7 and 8.2 μm, as well as a set of 4.3 μm CO_2 channels. The HIRS weighting functions are shown in Fig. 1, and appropriate channel information is listed in Table 1 (Smith *et al.*, 1975). In using the radiance information from these channels a priority system had to be followed. Groundwork for such methods is not new (Smith, 1970). All the radiative transfer details will not be given. Those modifications exclusive to this study will be explained below.

a. Relaxation equations

The 3.7 μm window channel was of primary importance in determining the background surface term in the radiative transfer calculations (Smith and Rao, 1973; Chahine *et al.*, 1977). This is especially true in determining moisture and temperature parameters from spectral regions with large transmittances at the surface (low atmospheric absorption).

The determination of the surface temperature, therefore, was the first step in the retrieval of atmospheric parameters at each scan spot of the satellite. For iteration $n + 1$

$$B(T_{\text{sfc}}^{(n+1)}, \nu) = B(T_{\text{sfc}}^{(n)}, \nu) + (R_{\text{obs}} - R_{\text{calc}}^{(n)})\tau_{\text{sfc}}^{-1}(\nu, T_0(p), Q_0(p)). \quad (1)$$

By inverting this equation we can see that the desired surface temperature $T_{\text{sfc}}^{(n+1)}$ in the Planck function B is the correct factor to make the calculated radiance R_{calc} in the window channel at wavenumber ν equal to the observed radiance R_{obs}. This assumes that the atmospheric temperature and moisture structure are either known or that unknown small differences are of minor significance. This idea, therefore, is to have good initial guess temperature $T_0(p)$ and mixing ratio $Q_0(p)$ profiles, where p is the vertical pressure coordinate divided into discrete levels, in order to initially determine the approximate atmospheric transmittance at the surface, τ_{sfc}. In the cases studied a composite of rawinsondes from a time period near the satellite

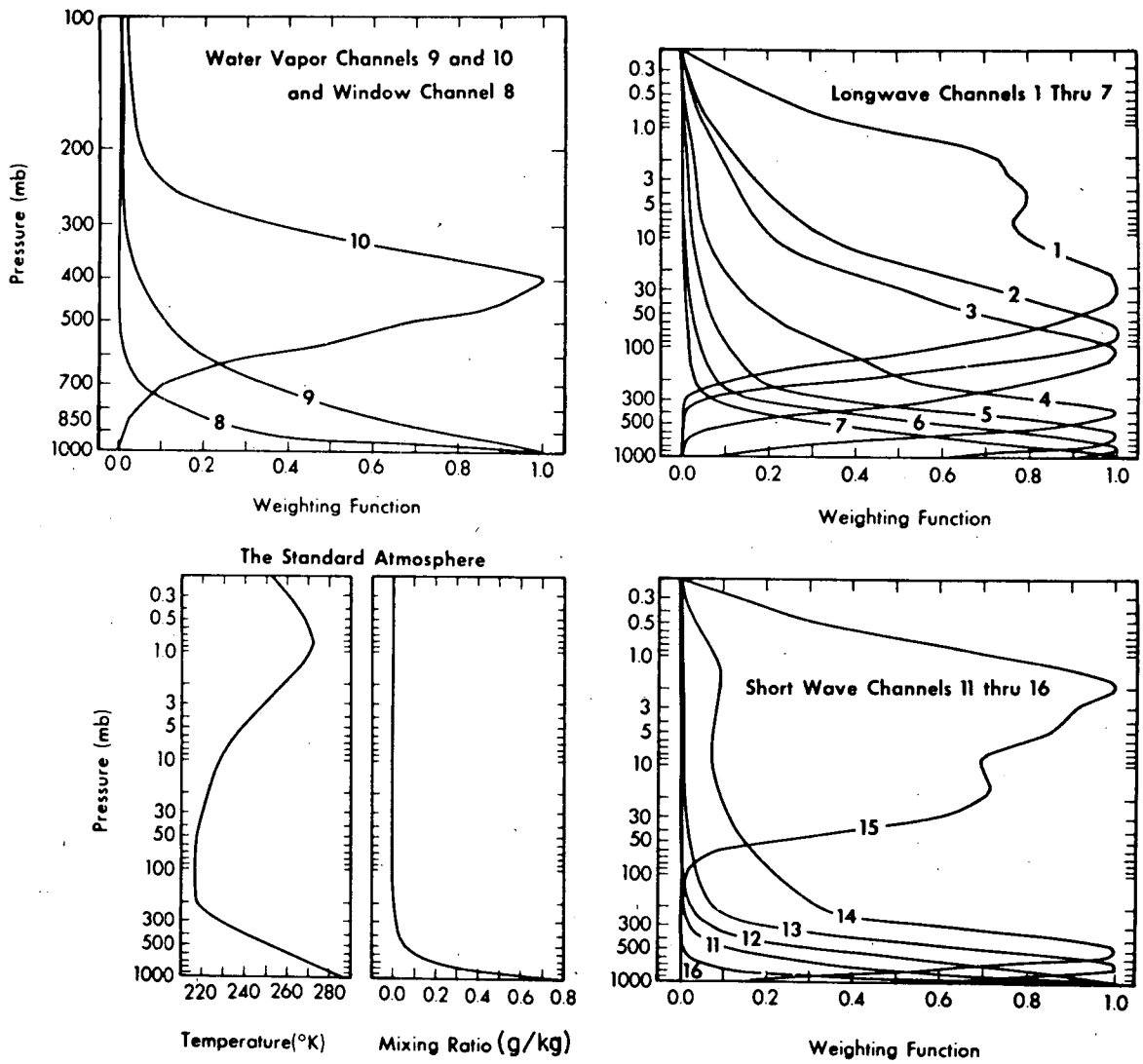

FIG. 1. Weighting functions for the HIRS water vapor and temperature channels.

pass was used as the initial guess, as will be explained later.

The second step was to adjust the initial guess moisture content and therefore the transmittances, according to the observed radiances in the 11 μm window channel and the two H_2O channels at 8.2 and 6.7 μm. This longwave window channel was used as a moisture sensing channel since its main absorbing medium in the clear atmosphere is water vapor.

Moisture feedback was accomplished through the relaxation formula for iteration $n + 1$:

$$Q^{(n+1)}(p) = Q^{(n)}(p)\left[1 - \sum_{i=1}^{3} \gamma_i \left(\frac{R_{\text{obs},i}}{R^{(n)}_{\text{calc},i}} - 1\right) \times W_i^{(n)}(p) \Big/ \sum_{i=1}^{3} W_i^{(n)}(p)\right]. \quad (2)$$

This applies to the mixing ratio $Q(p)$ at any discrete level p. A similar formula was used by Smith and Howell (1971) but was applied directly to the precipitable water integrated to any level p rather than the mixing ratio at that level. The longwave window and two H_2O channels are represented by the subscript i, and the weight W_i applied to each radiance channel and level is just the finite change in the transmittance at that level. Each radiance channel will perturb the mixing ratio profile $Q(p)$ at the pressure levels where its weighting function $W(p)$ is nonzero. The γ_i factors are necessary because of the change in units from radiance to mixing ratio. They approximate $(\Delta Q/Q)\cdot(R/\Delta R)$ or $\%\Delta Q/\%\Delta R$ (dimensionless). In the cases studied the γ_i factors which were used were calculated from the initial guess profile for each case study day. The calculated values will be listed in a later sec-

TABLE 1. Functions of the HIRS Channels

Channel Number	Channel Central Wave-number	Central Wavelength (μm)	Principal Absorbing Constit-uents	Level of Peak Energy Contri-bution	Purpose of the Radiance Observation
1	668	15.0	CO_2	30 mb	Temperature Sounding. The 15 μm band channels provide better sensitivity to the temperature of relatively cold regions of the atmosphere than can be achieved with the 4.3 μm band channels. Radiances in Channels 5, 6, and 7 are also used to calculate the heights and amounts of cloud within the HIRS field of view.
2	679	14.7	CO_2	60 mb	
3	690	14.4	CO_2	100 mb	
4	702	14.2	CO_2	250 mb	
5	716	14.0	CO_2	500 mb	
6	733	13.6	CO_2/H_2O	750 mb	
7	749	13.4	CO_2/H_2O	900 mb	
8	900	11.0	Window	Surface	Surface Temperature and cloud detection.
9	1224	8.2	H_2O	900 mb	Water Vapor Sounding. Provide water vapor corrections for CO_2 and window channels. The 6.7 μm channel is also used to detect thin cirrus cloud.
10	1496	6.7	H_2O	400 mb	
11	2190	4.57	N_2O	950 mb	Temperature Sounding. The 4.3 μm band channels provide better sensitivity to the temperature of relatively warm regions of the atmosphere than can be achieved with the 15 μm band channels. Also, the short-wavelength radiances are less sensitive to clouds than those for the 15 μm region.
12	2212	4.52	N_2O	850 mb	
13	2242	4.46	CO_2/N_2O	700 mb	
14	2275	4.40	CO_2/N_2O	600 mb	
15	2357	4.24	CO_2	5 mb	
16	2692	3.71	Window	Surface	Surface Temperature. Much less sensitive to clouds and H_2O than 11 μm window. Used with 11 μm channel to detect cloud contamination and derive surface temperature under partly cloudy sky conditions.
17	14,443	0.69	Window	Cloud	Cloud Detection. Used during the day with 3.7 μm and 11 μm window channels to define clear fields of view and to specify any reflected solar contributions to the 3.7 μm channel.

tion. The negative sign in Eq. (2) says that an increase in radiance is associated with a decrease in moisture.

The third step then involved adjusting the initial guess temperature profile according to the observed 4.3 μm CO_2 channel radiances. In a manner similar to moisture feedback, the temperature profile iterations followed a modified relaxation formula of Chahine (1968):

$$B(T^{(n+1)}(p), \nu) = B(T^{(n)}(p), \nu) \times\left[1 + \sum_{i=1}^{4}\left(\frac{R_{\text{obs},i}}{R^{(n)}_{\text{calc},i}} - 1\right) W_i^{(n)}(p) \Big/ \sum_{i=1}^{4} W_i^{(n)}(p)\right] . \quad (3)$$

For one channel this formula reduces directly to that used previously by the authors (Hillger and Vonder Haar, 1977, 1979) but the previous formula differed in that the resulting independent temperature determinations from each channel were weighted in a manner similar to the way the blackbody radiances are averaged here. This shortcut greatly reduced the number of calculations. The subscript i here denotes only the four most transparent 4.3 μm CO_2 absorption channels which were used to retrieve the lower tropospheric temperature profile for each scan spot. These four channels each have weighting function maxima below the tropopause, as do the channels which were used in the moisture relaxation equation.

The surface temperature, moisture and temperature iterative relaxation formulas [Eqs. (1), (2), and (3)] were applied in sequence as long as convergence was maintained. A decrease in the root-mean-square (rms) normalized radiance residual between observed and calculated radiances was the necessary criteria, i.e.,

$$r^{(n)}_{\text{rms}} = \left[\frac{1}{N}\sum_{i=1}^{N}\left(\frac{R_{\text{obs},i} - R^{(n)}_{\text{calc},i}}{R^{(n)}_{\text{calc},i}}\right)^2\right]^{1/2} . \quad (4)$$

The number of channels N included the two window, two H_2O and four CO_2 channels which were used in the retrieval process. The residuals were normalized to reduce the inequity caused by the different magnitudes of the radiances for various spectral channels. Usually as few as two or three complete cycles or iterations were required to obtain a moisture and temperature profile which provided radiances through radiative transfer calculations similar to those observed. This iterative scheme converged faster than previous methods applied to VTPR data (Hillger and Vonder Haar, 1977) since the transmittances were recalculated after the application of each iterative step.

b. Secondary mesoscale parameters

In addition to the surface temperature, mixing ratios and temperatures, which were retrieved directly from the satellite radiances, other mesoscale forecasting parameters also were calculated. Some of these parameters have fairly standard definitions and others were defined for this study.

The surface brightness (or interface) temperature calculated using Eq. (1) was considered to be independent of the air temperature of the lowest layer which was derived from Eq. (3). An equally weighted combination of these two temperatures was called the "sensible-heat" and was thought to be more closely related in some cases to the measured shelter temperature than either the surface interface or surface air temperature itself. Some discussion of this parameter will be given later.

For moisture parameters the directly retrieved mixing ratios were converted into dew point temperatures for comparison with the RAOB and surface observing networks. The most important secondary moisture parameter to be calculated was the total precipitable water. The precipitable water was determined by integrating the retrieved mixing ratio profile using

$$PW = g^{-1} \sum_{i=1}^{40} Q(p)\, \Delta p. \tag{5}$$

The summation is over the 40 pressure levels where the mixing-ratio profile was determined by iteration using the relaxation formula in Eq. (2). The total precipitable water gives a measure of the amount of latent energy available in the convective storm environment.

Likewise, atmospheric stability indices such as the total indices and K index have been used for many years (Miller, 1972) as good indicators of severe weather potential. These indices are measures of surface heating and moisture as well as atmospheric instability or the potential for release of such sources of sensible and latent energy.

Both the total indices and the K index are formed from differences between the dew point temperature at the 85 kPa level and the 50 kPa temperature. The K index also incorporates the 70 kPa temperature and dew point spread. Their formulas follow:

$$\text{Vertical-total} = T_{85} - T_{50}, \tag{6}$$

$$\text{Cross-total} = Td_{85} - T_{50}, \tag{7}$$

$$\text{Total-totals} = \text{Vertical total} + \text{Cross total}, \tag{8}$$

$$K \text{ index} = T_{85} + Td_{85} - (T_{70} - Td_{70}) - T_{50}. \tag{9}$$

Another combination moisture/stability parameter which was tested was labeled as "latent heat." This is the ratio of the total precipitable water to the surface mixing ratio [mm(g kg^{-1})$^{-1}$]. A change in this index or ratio would indicate changes in vertical moisture structure. Mixed results were obtained with this index, unlike the more standard stability indices given above.

The atmospheric stability indices that were calculated depend only on the temperature and moisture at various standard levels and are, therefore, static stability indices and not dynamic indices which incorporate air motions. The one-look of the satellite limits us to such static calculations. Neither the SWEAT (Severe Weather Threat) Index nor the SPOT (Surface Potential) Index (Miller and Maddox, 1975), for example, can be derived since the wind speed and direction at one or more levels are important factors in these more complex severe storm forecasting indices. Air motions would have to be implied or obtained from conventional surface or rawinsonde observation networks.

3. Corrections to HIRS radiances

a. Cloud detection

Cloud detection was accomplished using the visible (0.69 μm) and infrared window channels of HIRS. Cloudy fields-of-view (FOV's) were rejected, however, if the cloud cover exceeded 50% or if the clouds were determined to be cirrus. Cloud columns were always marked for possible future rejection if the derived parameters were not meteorologically consistent with surrounding clear columns. This reduced the possibility of cloud-induced biases in the resulting mesoscale fields.

Two methods were used for cloud detection. The visible channel of HIRS at 0.69 μm was used to sense reflected solar radiation from the surface of the earth or from clouds. If this visible channel radiance exceeded a 4.5 mW (m^2 sr cm^{-1})$^{-1}$ threshold, clouds were assumed. On the chosen days a maximum 0.69 μm radiance of ~22 mW (m^2 sr cm^{-1})$^{-1}$ was detected, and theoretical calculations indicated that this value would be equivalent to an isotropic surface reflectivity or albedo of unity. Thus the 4.5 value represents an albedo of ~20% if the instru-

ment response is linear with cloud amount. This threshold was also empirically found to be a good threshold by comparison with clouds seen in concurrent Synchronous Meteorological Satellite (SMS) visible images on the days examined.

A second and more rigorous method for detection of clouds or inhomogeneous surface characteristics was also used. This method relied on the fact that the two HIRS window channels at 3.7 and 11 μm respond as different powers of effective temperature. A uniform FOV in the sounded column would produce an equivalent radiative temperature in each channel, but an inhomogeneous FOV would produce different radiative temperatures (Smith and Rao, 1973; Smith *et al.*, 1974). The difference in effective temperatures between the two window channels was allowed to be as great as 11.5 K before clouds were considered to have contaminated the field-of-view. This rather large difference allows for the differing atmospheric absorption and emission characteristics in each spectral interval. This method was used to detect cloudy FOV's that were not normally detected by by reflected radiation method, such as occurs in the case of small cloud amounts or thin cirrus clouds (Shen and Smith, 1973).

If clouds were detected by either method the cloud amount was assumed to be proportional to the 0.69 μm radiance (or the albedo). Cloud pressure was then calculated as a minimum in radiance residuals using the 15 μm CO_2 channels, in a method similar to that used in previous work (Hillger and Vonder Haar, 1977). Cloudy FOV's were thereby proportioned into a clear and cloudy fraction. Details can be found in Shaw *et al.* (1970).

b. Solar correction to shortwave channels

The reflected radiation in the 0.69 μm visible channel was also used to determine the amount of reflected radiation in the 3.7 μm IR window channel, the shortwave 4.3 μm CO_2 channels, and the H_2O channels. The maximum possible solar contamination in each of these IR channels was prorated by the ratio of the reflected energy in the visible channel to its theoretical maximum as was similarly done above to find the cloud amount for cloudy FOV's:

$$\left.\begin{aligned} SC_i &= S_i \cdot \mathrm{Alb} \cdot \tau^{(\sec\Phi_0 + \sec\Theta)} \\ \mathrm{Alb} &= \frac{R(0.69\ \mu\mathrm{m})}{22\ \mathrm{mW}} \end{aligned}\right\} . \qquad (10)$$

This ratio or albedo was assumed constant across the short-wavelength IR spectrum. The maximum solar contamination S for each channel i was also reduced by the atmospheric transmission τ. In the case of reflected radiation the atmosphere path is transversed twice. The Φ and Θ angles are the solar and satellite-view zenith angles, respectively.

Since the albedo in most non-cloudy cases was on the order of 10–15%, the solar correction was typically ~0.2 mW $(m^2\ sr\ cm^{-1})^{-1}$ for the 3.7 μm window. Other channels had less reflected radiation and smaller solar corrections. The visible channel, therefore, allowed a simple correction for reflected radiation in the other shortwave channels.

c. Surface elevation and viewing angle corrections

A major correction to the radiative transfer calculations was necessary for surface elevations or pressures other than sea level. This was especially true for the western regions of the area of study where the surface pressure approximated the 85 kPa level. Therefore, each satellite retrieval utilized a look-up table of mean surface elevation to determine the lower boundary in that column. The mean surface elevation was known for every 0.5° of latitude or longitude, and the 1962 Standard Atmosphere was used to find the equivalent surface pressure.

The scan pattern of HIRS allowed for solar zenith angles ranging from 0 to 45°. These changes were incorporated into the radiative transfer equation through transmittance calculations which were a function of the HIRS viewing angle. Thus, as was similarly done for the surface elevation, rather than trying to adjust the observed radiances to a common viewing angle (nadir) and surface pressure (sea level), the calculated radiances incorporated the viewing angle and surface pressure corrections.

4. HIRS satellite data

a. Case study days

The first HIRS radiances available for study were obtained during the data systems test (DST) period in August and September of 1975 (Gary, 1977). This was shortly after the launch of Nimbus 6. Of these days, only four were available over the region of study with near-nadir views. The sub-satellite tracks on these four days are shown in Fig. 2 along with the boundary for the study area which is centered on the SESAME mesoscale sounding network in western Oklahoma. The size of the region for study was chosen to be 10° latitude × 10° longitude (30–40°N and 95–105°W). This represents an area of ~1000 km on a side. This size allows a study of mesoscale weather over a large region covering most of Kansas, Oklahoma and northern Texas. The state outlines are shown along with the NWS sounding network within and around the study area. These RAOB's were used to calculate the initial guess temperature and moisture profiles that were needed for each case study day.

Nimbus 6 is a polar-orbiting satellite with an ascending daytime orbit. Over the region of study

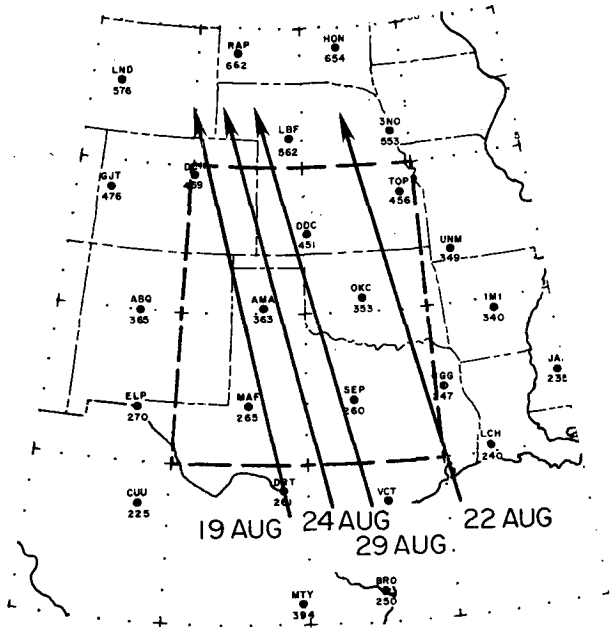

FIG. 2. HIRS sub-satellite tracks over the region of study.

the time of satellite coverage occurs at approximately 1800 GMT (1200 CST or local noon). This time frame typically provides a cloud-free indication of midday weather before subsequent convective activity occurs later in the day. Radiances for each spectral interval were sensed in 21 spots on each side of the subsatellite track at a resolution of ~30 km at nadir. Only the spots which fall within the specified boundary were analyzed. Coverage was continuous except during calibration periods of the satellite which occur every 20 scan lines.

b. Initial guess profiles and moisture feedback

For each case study day one initial guess sounding was used for the entire field of HIRS radiances. The initial guess was a composite (mean) of all available RAOB temperature and moisture profiles for a synoptic sounding time near the satellite pass. In all cases the initial guess profile was a composite of the 0000 GMT RAOB's, 6 h after the local noon (1800 GMT) satellite pass. The 0000 GMT soundings were chosen rather than the 1200 GMT soundings since the early morning 1200 GMT soundings in many cases contained temperature inversions near the surface. If a profile with a temperature inversion was used as an initial guess then a temperature inversion would continue to show up in the retrieved soundings. The vertical resolution of the satellite sounder is not sufficient to smooth out or add features of such fine vertical structure. However, using 0000 GMT soundings is not a limitation since the initial guess profiles for each case study day were similar and soundings from 0000 GMT the previous day could just as easily have been used.

It must be emphasized that there was only one initial guess created for each case study day and all retrieved soundings produced on that day used that same initial guess profile. Therefore, all horizontal structure that showed up in the retrieval fields was due only to the structure in the measured radiances from the satellite.

As shown in Table 2, each initial guess sounding contained ~38 mm of precipitable water and had a surface temperature near 34°C. These soundings could probably have been replaced by one initial guess profile for the entire period. That would not have been feasible, however, if the case study days occurred in different seasons of the year. All cases studied here were in August with nearly similar composite surface and upper air structures.

These initial guess profiles were used to assure that the weighting functions for each channel were correctly initialized. After each iteration the transmittances were recalculated to reflect the changed temperature and moisture profiles. The initial guess, therefore, played only a minor role in starting the iterative process. The major contribution of the initial guess profile was to determine the moisture feedback parameters (γ_i) used in Eq. (2). The last three columns of Table 2 show the calculated feedback values which were used for each case study day for the 11 μm window and the two H_2O channels. The most transparent channel at 11 μm had the largest feedback values. This is because the weighting function for this channel does have its maximum nearer the surface where the amount of atmospheric moisture is greatest. The average feedback values

TABLE 2. Initial guess sample values and the resulting calculated moisture feedback values.

Date	Sample values		Moisture feedback values		
	Precipitable water (mm)	Surface temperature (°C)	Ch 8 (11 μm)	Ch 9 (8.2 μm)	Ch 10 (6.7 μm)
19 Aug 1975	37.2	33.6	7.3	4.9	3.4
22 Aug 1975	39.4	33.9	7.0	4.8	3.4
24 Aug 1975	38.9	36.7	5.6	4.1	3.5
29 Aug 1975	37.6	34.2	6.6	4.7	3.4

TABLE 3. Composite comparisons of satellite-derived parameters with RAOB's and surface observations for the four case study days.

Satellite-derived parameter at ~1800 GMT	1800 GMT interpolated RAOB[a]			1800 GMT synoptic surface observations[b]		
	Correlation	Bias	rms difference	Correlation	Bias	rms difference
Temperature						
surface (°C)	0.70	4.2	5.4	0.36	−0.6	2.7
85 kPa (°C)	0.77	2.7	3.4			
70 kPa (°C)	0.75	1.2	1.6			
50 kPa (°C)	−0.12	1.3	2.0			
30 kPa (°C)	−0.25	1.4	1.9			
Brightness temperature T_B (°C)	(0.32)[c]	(14.6)[c]	(16.3)[c]	(0.32)[d]	(11.3)[d]	(12.5)[d]
Sensible heat (°C)	(0.59)[c]	(9.7)[c]	(10.2)[c]	(0.48)[d]	(5.4)[d]	(6.0)[d]
Total PW (mm)	0.89	−0.2	5.5	(0.83)[e]		
Dew point temperature						
surface (°C)	0.97	−1.0	2.5	0.87	−2.4	4.0
85 (°C)	0.81	−1.0	3.3	(0.85)[e]		
70 (°C)	0.37	0.2	3.8			
Cross total (K)	0.79	−2.3	4.4			
Total total (K)	−0.01	−0.5	5.5			
K index (°C)	0.49	−0.3	7.3	(0.85)[e]		
Latent heat [mm(g kg^{-1})$^{-1}$]	0.37	0.02	0.28	(0.67)[e]		

[a] Based on a minimum of seven pairs per day.
[b] Based on a minimum of 25 pairs per day.
[c] Compared to RAOB surface temperature.
[d] Compared to synoptic surface temperature.
[e] Correlation with synoptic surface dew point temperature.

were approximately 6.6, 4.6 and 3.4 for channels 8, 9 and 10, respectively. The details of the feedback calculation are outlined by Smith (1970).

5. Analysis of satellite-derived parameters

The parameters resulting from the HIRS moisture-temperature retrieval process will be analyzed three different ways. The first analysis gives the standard numerical correlations and differences when the satellite-derived parameters are compared to the same or similar parameters from both RAOB's and also to higher resolution synoptic surface observations. A second analysis shows the individual case study comparisons of the satellite-derived surface dew point fields to the same fields constructed from synoptic surface observation. Some examples of static stability fields also will be shown for comparison with later convective development. A third analysis of the satellite-derived parameters is a statistical structure analysis of "signal" and "noise" levels of the various fields to see for which parameters the information content is greatest.

a. Comparison to conventional measurement systems

The parameters derived from the Nimbus 6 HIRS radiances are listed in Table 3. The correlations and mean and rms differences listed are a composite of the results for all four case study days. Some individual parameter comparisons will be shown later. The satellite-derived parameters were compared to two different conventional data sets. One set was the same parameters derived from RAOB's in the area of study which were time-interpolated to the satellite time. The other conventional data set included all synoptic surface observations within the region of study. These surface observations of dew point and temperature were taken at the same approximate local noon time as the satellite pass.

The numerical comparisons in the first three columns of Table 3 were calculated from a pairing of the HIRS-derived values with the equivalent values from conventional RAOB measurements. All satellite-derived values within a 32 km radius of each rawinsonde site were averaged for the comparison with the RAOB values. This average included up to four individual satellite soundings. The RAOB values were time-interpolated to 1800 GMT from the bordering synoptic NWS rawinsonde sounding times of 1200 GMT (6 h before the satellite pass) and 0000 GMT (6 h after). The number of RAOB's for comparison was a minimum of seven, one for each rawinsonde site within the region of study. This is a small number of samples for comparison. Therefore, these results should not be generalized. In spite of this, the correlations (cross products of the differences about each sample mean) were fairly high especially for the total precipitable water and surface dew-point temperature. In these cases the satellite-derived values explained at least 80% of the variance of the equivalent RAOB values. Other parameters showed lower correlations with the RAOB's since some of these were secondary prod-

ucts of the retrieval process, the main goal of which was to derive lower tropospheric parameters, especially moisture. Even in the case of total precipitable water, the majority of the moisture resides near the surface.

The mean satellite-RAOB differences (biases) and rms differences are shown in columns 2 and 3. The satellite-derived temperature values were biased too warm compared to the RAOB values and the moisture values derived from HIRS radiances are slightly too dry. This bias is no big problem and can be easily taken out in such a comparison. The rms differences were only slightly larger for most comparisons, but the static stability parameters showed the largest rms differences. This is probably due to their vertical differencing nature which is a weak point in satellite soundings which have inherently low vertical resolution. Vertical integration, on the other hand, such as used in the total precipitable water calculation, did also give a relatively large rms difference in comparison to RAOB's, but the precipitable water correlation was still high.

The large mean and rms differences for the surface brightness temperature and "sensible-heat" parameters were due to the surface brightness temperatures being much warmer than the actual shelter temperatures. These parameters were calculated to see if they provided better comparisons with the shelter temperature than the air temperature derived from the HIRS CO_2 channels. The brightness temperature is related to the window channel radiance corrected for atmospheric transmission, and the "sensible heat" is the mean of that value with the surface temperature from the CO_2 channels. Neither of these values provided a better correlation with the surface temperature in this comparison with RAOB values.

The last three columns show a similar comparison of some of the same satellite-derived parameters with the time-coincident synoptic surface observations of temperature and dew point. Again the correlation was highest for the surface dew-point temperature. Other satellite-derived values were compared to either the surface temperature or dew point since brightness temperature, precipitable water and stability indices are not part of the 3 h synoptic surface observation network. The rather high correlation of the satellite-derived static stability indices with the surface dew point shows the strength of the lower tropospheric moisture in these stability calculations.

The comparisons with the synoptic surface observations included a minimum of 25 pairs of values, so these results carry more weight. The bias values again showed that the satellite-derived surface dew-point temperatures were in general too low (too dry), but the rms differences for both surface temperature and dew point are very reasonable. The "sensible-heat" parameter also shows a rather large bias but a better correlation with the synoptic shelter temperature than either the CO_2 surface temperature or the surface brightness temperature. Thus this parameter does have some merit when compared to synoptic shelter temperatures.

b. Individual case study days

Three of the four case study days will be discussed in detail in the following sections. Not all satellite-derived analysis and forecasting parameters will be shown for each day. Rather, a few selected analyses will be discussed, especially those which show more interesting meteorological features. The satellite-derived fields will focus on these features and show comparison to fields of conventional surface observations. The surface dew-point temperature analyses will be emphasized since equivalent fields are available from surface observations taken at the same time.

1) 22 AUGUST 1975

Unlike 19 August (not discussed) which produced little or no convection in the region of study, this day produced some rather large convective regions in northwestern Kansas and central Oklahoma. The central Oklahoma region will be focused on to show that the satellite-derived surface dew-point temperature analysis does contain a feature which is hidden at even the synoptic surface observation scale. The satellite-derived dew-point analysis at 1743 GMT (approximately local noon) in Fig. 3a shows a relatively moist tongue through central Oklahoma. Dew points above 22°C at the surface indicate the presence of a moist pocket compared to relatively drier regions to the east and west. This same region is outlined in the 1800 GMT synoptic surface dew-point analysis in Fig. 3b. Dew points here are also above 22°C, but the drying to the east is not indicated. This same feature also shows up in the satellite-derived total PW field and the static stability fields (not shown). This seems reasonable, since these secondary fields are highly dependent on the surface moisture field. The wind barbs in Fig. 3b also indicate that the flow of moisture is from the south, so such a moist tongue could be expected.

One proof of this moisture tongue can be seen in the developed convection in the 2145 GMT SMS visible image in Fig. 3c. The line of convection from east central Texas up into central Oklahoma is clearly shown here. The convection in Oklahoma first appeared on the radar summary at 2035 GMT (not shown). The only severe weather report, however, was a windstorm in the region of northern Texas near the Oklahoma border (*Storm Data*, 1975). That windstorm occurred at about 2000 GMT,

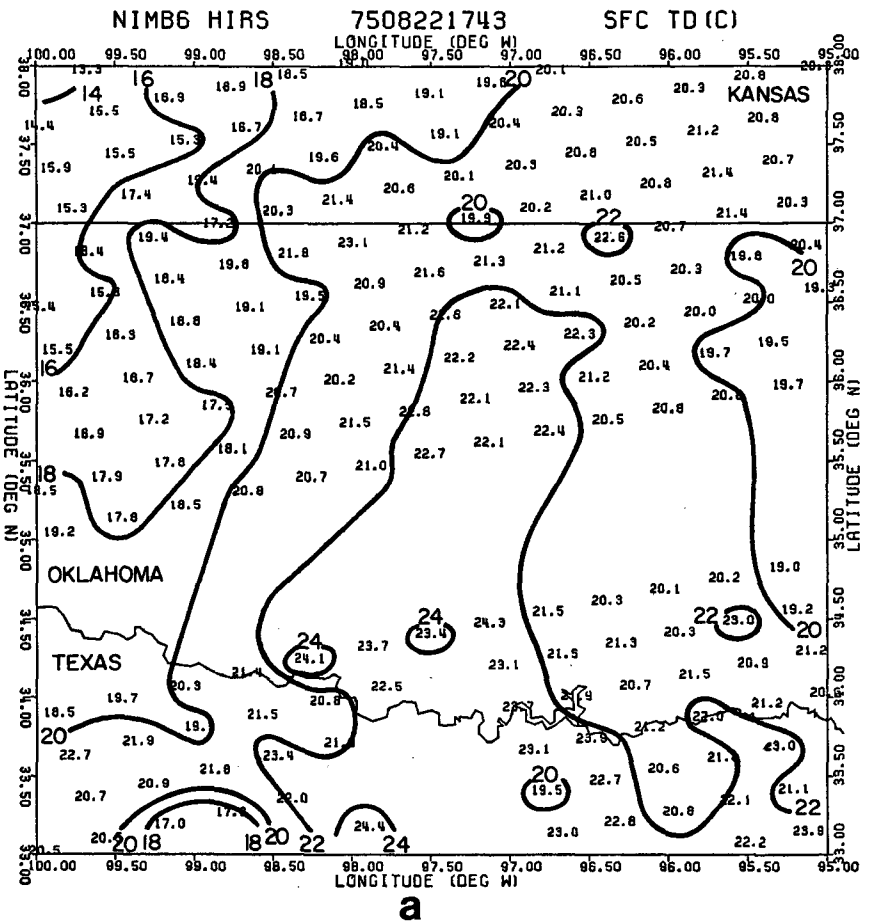

FIG. 3a. Satellite-derived surface dew-point temperature analysis for 1743 GMT 22 August 1975. Contours are every 2°C.

about 2 h after the local noon satellite analysis, and very near 33.5°N, 97°W.

The SMS visible image at 1800 GMT in Fig. 3d (~15 min after the HIRS measurements) shows that there appears to be no indication of cloudiness in central Oklahoma at the time of the satellite measurements. The cloudy region in Texas is the only indication of southerly moist flow off the Gulf. The satellite-derived moisture field, however, does show a significant moisture feature in central Oklahoma at least 2 h before the first convection occurs in that region.

An indication of the effect of clouds on the satellite-derived analysis is given by a few noisy values in northern Texas in Fig. 3a. Some satellite-derived surface dew points are too low compared to surrounding values. This high spatially irregular noise is easily picked out since clouds are seldom very uniform. Individual values which are not meteorologically consistent with their surroundings should therefore be eliminated. However, larger features such as the moist tongue in central Oklahoma which are more uniform were shown not to be cloud induced.

2) 24 AUGUST 1975

This next case study day was characterized by much more suppressed convective activity, with only very isolated cells. The subsequent convection occurred in the Texas panhandle which will be the focus of the satellite-derived fields to the exclusion of the larger gradient of moist to dry generally from east to west.

Fig. 4a shows the satellite-derived surface dew point analysis at 1801 GMT (local noon). The general moisture gradient is offset by a local maximum in the southwestern part of the Texas panhandle. Dew point temperatures are above 14°C there compared to drier regions around. This local maximum is not shown in the 1800 GMT synoptic surface dew point analysis in Fig. 4b. The only indication of extra moisture in this region may be the bulge in the 14 and 16°C dew point lines where they penetrate southeast New Mexico.

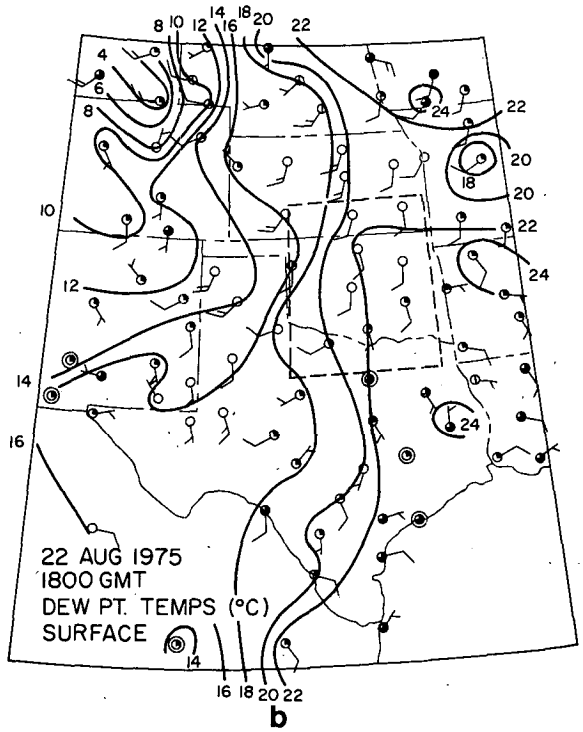

FIG. 3b. Conventional synoptic surface dew-point temperature analysis (°C) at 1800 GMT 22 August 1975. Contours are every 2°C.

Convection does occur in this region, as seen in the SMS visible image at 2030 GMT in Fig. 4c. This image occurred 2.5 h after the satellite-derived measurements and is coincident with the first radar-observed convection at 2035 GMT (not shown).

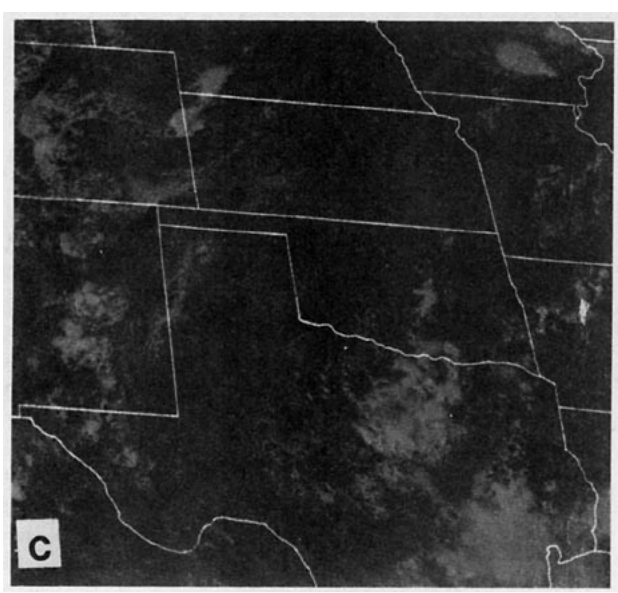

FIG. 3c. SMS visible image at 2145 GMT 22 August 1975.

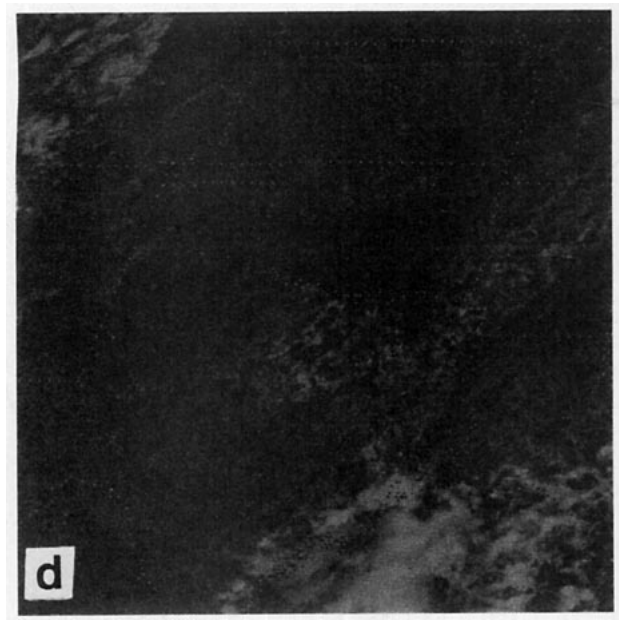

FIG. 3d. SMS visible image at 1800 GMT 22 August 1975.

The cross-total stability index for this same area in Fig. 4d shows a field with more pronounced features than the dew point analysis. The local maximum of instability in the Texas panhandle is distinctly separated from more stable surrounding areas. Also, the tight gradient to the northeast does correspond to the convective line which later developed up through the Texas panhandle. This tight gradient is not observed as readily in the dew-point analysis. This stability analysis, therefore, shows a strong relationship to the convective line which formed 2.5 h later.

A direct comparison of the satellite-derived surface dew-point temperatures with the closest synoptic surface dew-point temperatures is shown in Fig. 5. The graph shows a point-to-point correlation of 0.90 (81% explained variance). The center line represents a one-to-one correlation and the dashed lines outline the spread of the data. The satellite-derived dew points are biased too low since most of the points lie below the center line. This remained true in the composite results in Table 3 which showed a mean bias of -2.4 K for all case study days. Besides the bias, the difference between the two sets of measurements seems to be greater for small dew points (dry areas) and less for moist areas. Generally, the difference appears to be a maximum of 8 K with much smaller differences typical. It should be pointed out that this difference is not entirely an error in the satellite-derived dew points but is also the error in the synoptic dew points since neither set is error-free. Sampling differences also account for some of the variation, but generally the two sets show very similar results. Even the partly

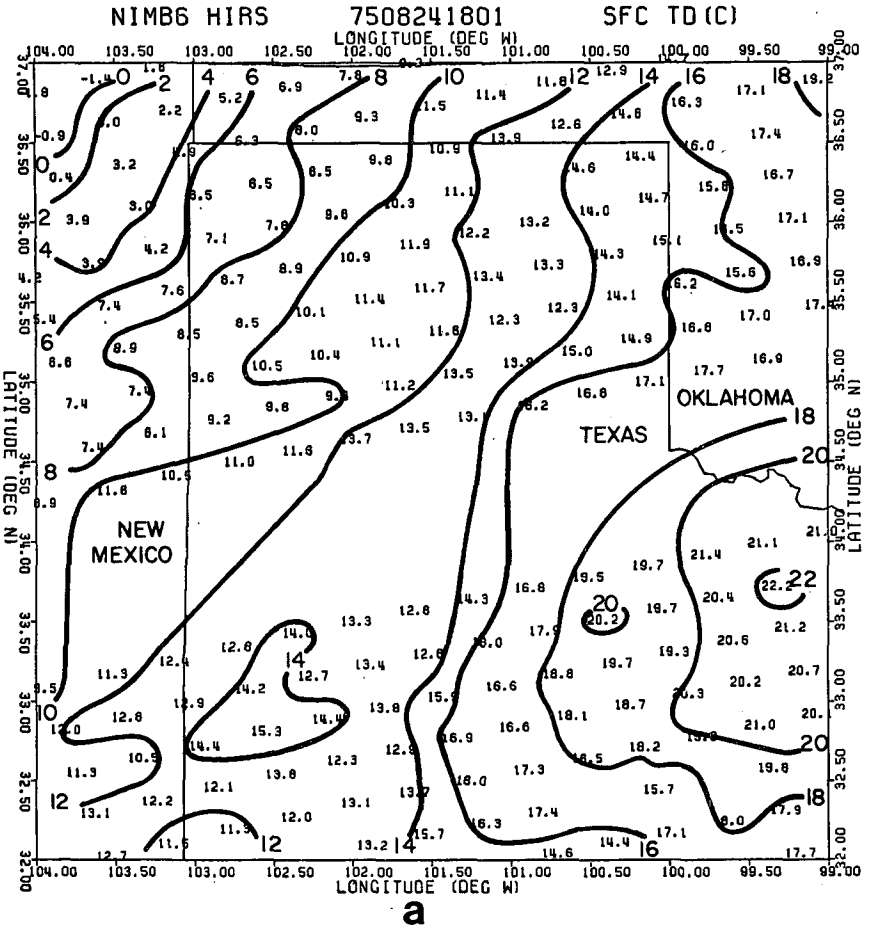

FIG. 4a. Satellite-derived surface dew-point temperature analysis (°C) for 1801 GMT 24 August 1975. Contours are every 2°C.

cloudy values (circles) do not deviate abnormally from the clear values.

3) 29 AUGUST 1975

This last case study day was perhaps the most interesting. Convection occurred in southwestern Kansas and the Oklahoma panhandle for several hours after the satellite pass. The satellite-derived surface dew-point temperature analysis at 1757 GMT in Fig. 6a shows both tongues of moist and dry air. These features distort the moisture field which is normally thought to be uniform and smooth. The same area is outlined in the 1800 GMT synoptic surface dew-point analysis in Fig. 6b. Here the tightest moisture gradient appears to be toward the western side of the area of study, but it is still rather smooth. Much less mesoscale detail is given with this data set.

This strong gradient is probably the best indication of the dry line feature which frequently exists in the high plains during many days in the summer (Rhea, 1966). Schaefer (1973, 1974) defined the dry line as the 9 g kg^{-1} mixing ratio line which is consistently near the center of the zone of sharpest mixing ratio gradient. The equivalent dew-point temperature at the surface for saturation at 9 g kg^{-1} is about 12°C.

The 12°C dew-point line as shown in the satellite analysis has two major features which are associated with later convection. These are the larger moist tongue in western Kansas and the smaller moist tongue in the Oklahoma Panhandle. These are separated by a relatively dry tongue extending from southeast Colorado into southwestern Kansas. These two moist tongues are associated with areas of subsequent convection. To show this convection a composite radar summary is given in Fig. 6c. This composite was constructed from hourly radar summaries from 2035 GMT, when the first echoes appeared, until 0335 GMT. Shading was used to indicate the duration of the convection, with the darkest shading representing echoes which lasted 2 h or more. Some selected echo tops and their times of occurrence are also pointed out.

The dry tongue in southwestern Kansas as pointed

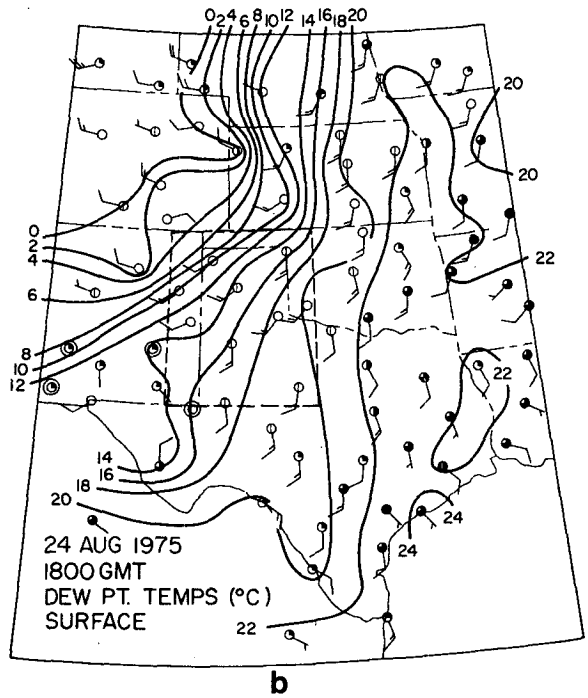

FIG. 4b. Conventional synoptic surface dew-point temperature analysis (°C) at 1800 GMT 24 August 1975. Contours are every 2°C.

out in the satellite-derived dew-point field separates the two main areas of convection. This same dry feature is not evident in the synoptic analysis. The lower resolution of the surface observations is not adequate to pick out such detail.

The satellite-derived K index analysis shown in Fig. 6d confirms the dew point analysis. Areas of higher instability are also aligned with the later convective areas and the dry tongue has much lower instability values. These stability values are strongly dependent on the moisture analysis but also take into consideration the temperature parameters. Therefore, the analysis is not identical to that of moisture. Both the moisture and stability fields, especially when looked at together, do give a good indication of the most likely areas for convection to occur, as happened 2.5 h later. The significance of the satellite-derived fields is their high-resolution capability to pick out perturbations on a normally much smoother picture from just surface observations. The surface observations do pick out the general dry line position and the increasing moisture to the southeast which is typical in this region for all months of the year (Reitan, 1960), especially the summer. But the true moisture structure is the key to mesoscale forecasting.

c. Structure function analysis

Structure analysis as used here gives a statistical measure of the quality of the satellite-derived parameters. This statistical measure is independent of any satellite-RAOB comparison since only satellite-derived values are used. Each case study day was analyzed and the results were again composited as was done for the satellite-RAOB comparisons.

"Noise" levels were obtained for each variable from a structure function analysis (Gandin, 1963) of all the satellite-derived values in the area of study. The analysis method was the same as that used by the authors in a previous study of VTPR satellite soundings (Hillger and Vonder Haar, 1979). The theory behind determining the "noise" level for closely spaced data is to extrapolate the statistical difference between the individual measurements as the separation between the measurements is decreased. This statistical rms difference should decrease as individual measurements are more closely separated. At some distance the mean gradient should disappear and only the noise in the individual measurements should remain. In the case of the HIRS radiances the closest measurements are separated by ~30 km minimum. Some mean gradient would generally exist in the measurements at this distance and only an extrapolation to zero separation distance would eliminate this gradient. However, the reason for not extrapolating is that there is no assurance that the statistical difference between the measurements will decrease beyond its value at this minimum separation distance. In other words, the intrinsic noise level may have been obtained regardless of how closely spaced the measurements were made. The rms difference at this minimum separation distance is then assumed to be a measure of the "noise" level of the satellite-derived parameters.

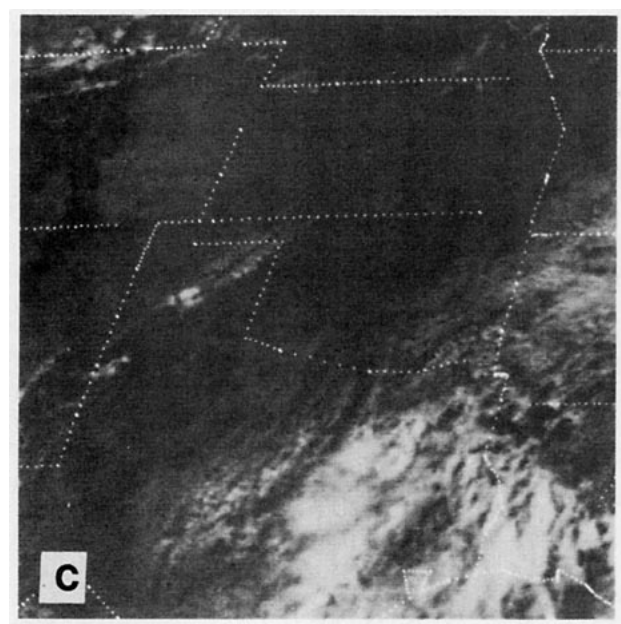

FIG. 4c. SMS visible image at 2030 GMT 24 August 1975.

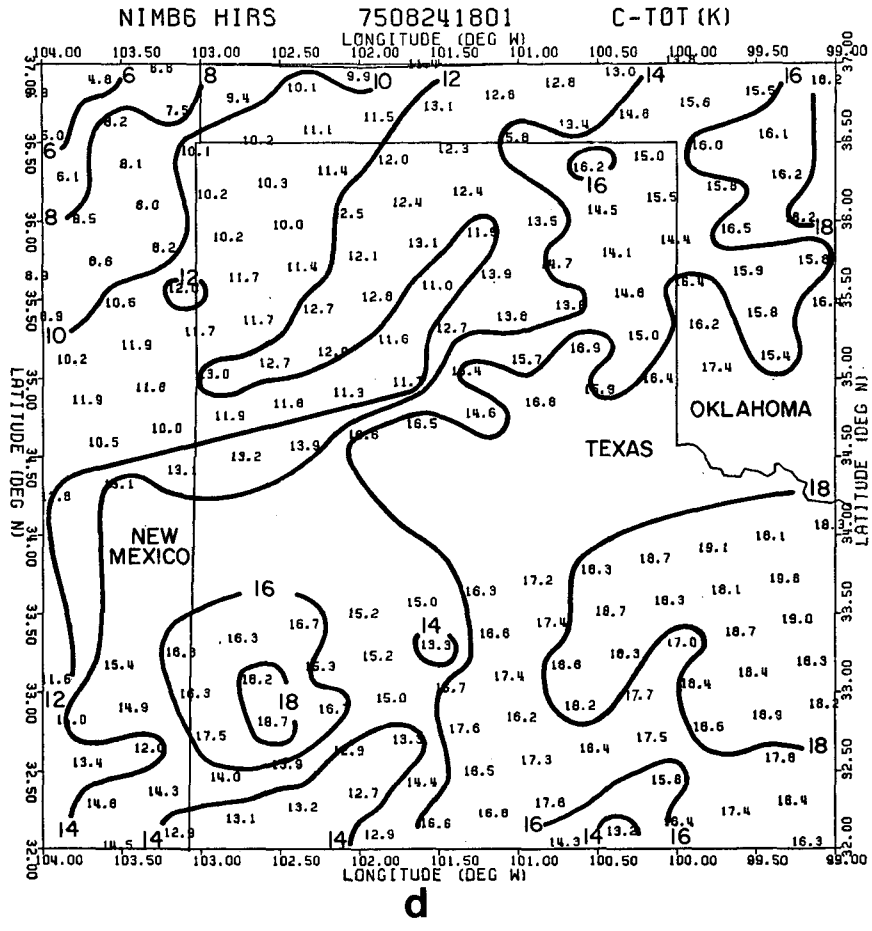

FIG. 4d. Satellite-derived cross-total stability analysis (K) for 1801 GMT 24 August 1975. Contours are every 2 K.

Table 4 shows the rms "noise" levels obtained for the same parameters as used in the satellite-RAOB comparison. The minimum separation between adjacent HIRS measurements averages ~33 km. The approximately 200 samples for each case study day provided ~400 sets of paired values at this minimum separation. Column 1 shows that temperatures at the five levels examined were typically obtained with rms "noise" levels of less than 1 K. Similarly, for moisture the "noise" levels were less than 2 mm of H_2O for total precipitable water and less than 1.5 K for dew-point temperatures. Other parameters showed higher rms "noise" levels, but none of the results were unreasonable. These statistical values may mask some larger differences between individual adjacent paired measurements, but the results are as good as can be expected from an equivalent RAOB network measuring at the same resolution.

To put these "noise" levels into better perspective, they should be compared to the standard deviation of all the measurements in the individual fields. The standard deviations in column 2 of Table 4

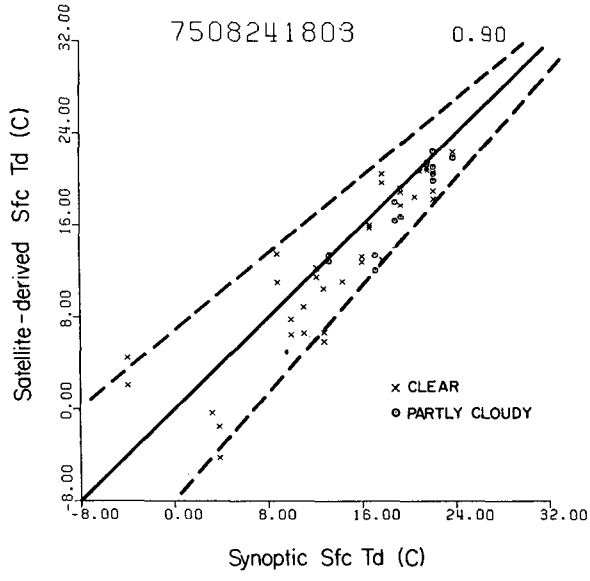

FIG. 5. Scatter plot of satellite-derived surface dew-point temperatures versus conventional synoptic dew-point temperatures for 1800 GMT 24 August 1975.

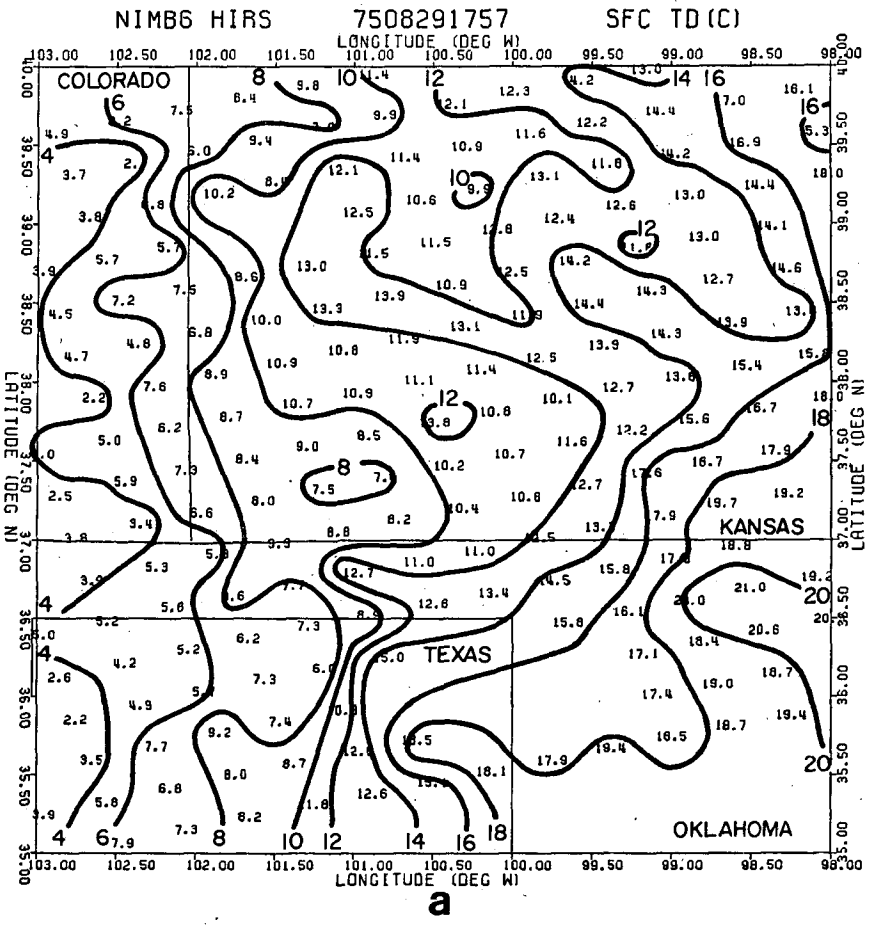

FIG. 6a. Satellite-derived surface dew-point temperature analysis (°C) for 1757 GMT 29 August 1975. Contours are every 2°C.

show the amount of variability in the derived fields. The amount of variability depends on both the true variability and the ability to detect that variability, such as gradients in the field. Only if the variability is larger than the "noise" level for that field will there be significant information in the field, unless, of course, if the true field is flat. Column 3 lists the "signal" to "noise" ratios of the previous two columns. There appears to be significant signal above noise at the mesoscale for all variables except for some of the non-surface temperature fields and the latent-heat index. For these variables the signal-to-noise ratio is <2. These results point to a decreased temperature retrieval ability when compared to the signal above noise for the moisture variables. This is possibly due to the iterative moisture-temperature retrieval scheme design which adjusts the initial guess moisture before the temperatures are adjusted. This would make the moisture signal improve at the expense of the temperature signal. Another explanation is that there is basically much more moisture signal in mesoscale situations than there is a temperature signal, so the order of the iterations may be justified.

The low "signal-to-noise" ratio for the latent heat index does indicate some lack of vertical resolution in the satellite-derived moisture. A much higher ratio would be expected if this parameter were to pick up horizontal variations in the vertical moisture structure. Also, the satellite-RAOB comparison in Table 3 did show that this latent heat parameter was not correlated very well with the RAOB measurements. However, none of the parameters had noise levels equal to or greater than the signal. Otherwise there would be no information content in those variables.

6. Summary and conclusions

Possibly some of the biggest strides in weather analysis and forecasting in the next few years will be at the mesoscale (25–250 km). This scale deals with

the environmental conditions around convective storms or systems of such storms. Features to be studied usually have some type of organization such as along a dry line or mesoscale frontal feature. The actual moisture and temperature structure of those mesoscale features may not be very well known. Therefore, the recent emphasis is on programs such as SESAME which call for both this type of mesoscale investigation of severe storm situations and a study of new tools such as the satellite sounder which can provide high-resolution measurements over areas of interest.

The HIRS satellite soundings in this study were used at their full resolution of 30 km (barring clouds). Radiances from the HIRS instrument were used in a mesoscale moisture-temperature retrieval scheme to produce fields of mesoscale analysis and forecasting parameters necessary for pre-convective research. This moisture-temperature retrieval scheme was designed specially to extract lower tropospheric temperatures, dew point temperatures and stability indices. These satellite-derived parameters were then analyzed three different ways.

One analysis of the satellite-derived parameters was a direct comparison with RAOB's and surface observations. The comparison to both sets of conventional observations gave the highest correlations for the moisture parameters, but also high correlations for the lower troposphere temperature parameters. Mean differences indicated that the satellite-derived moisture was slightly too low compared to RAOB's, but this is no real problem since the relative change in the horizontal is of major concern. Rms differences were also very reasonable when it is remembered that two different measurement systems are being compared.

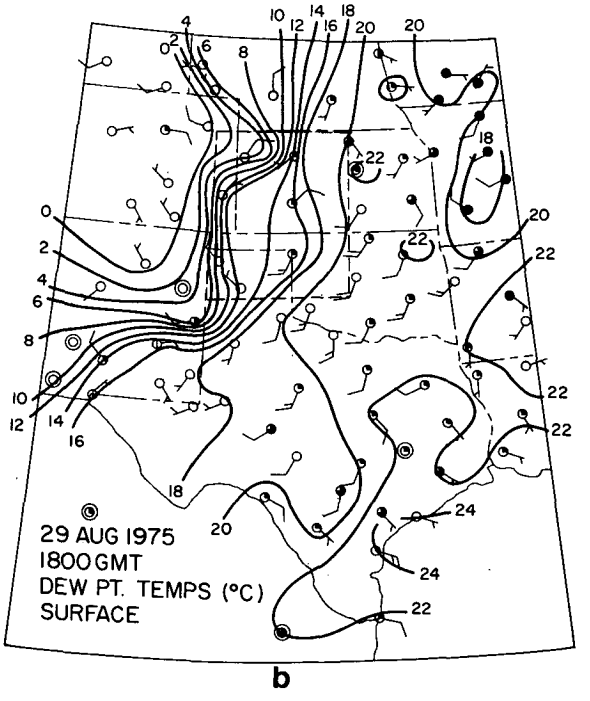

FIG. 6b. Conventional synoptic dew point temperature analysis (°C) at 1800 GMT 29 August 1975. Contours are every 2°C.

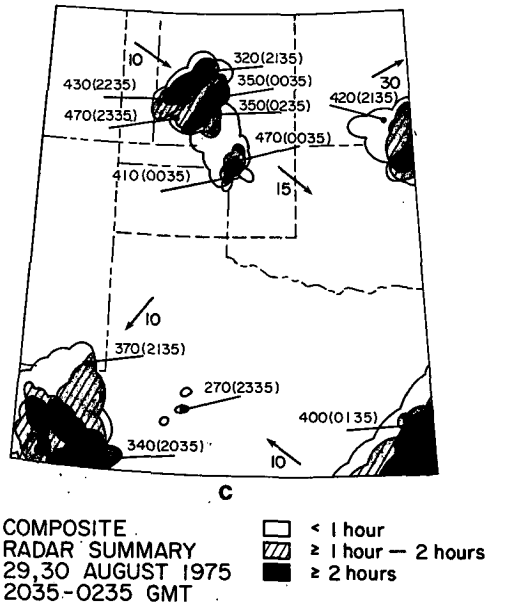

FIG. 6c. Composite radar summary from 2035 GMT (29 August 1975) to 0235 GMT (30 August 1975).

The second analysis was an individual case study test of satellite-derived fields. In each of these cases the satellite-derived surface dew point field for a selected sub-area was compared to the synoptic surface observations. None of the case study days provided any extremely severe weather. Most development was merely medium sized convection due to suppressed conditions. The convection, however, did tend to form in conjunction with mesoscale features associated with the dry line or in relation to moist and dry tongues from differing air masses. These features were sometimes also identified in the synoptic surface observations, but were given much more detail in the higher resolution satellite soundings. The idea was to have the ability to better pinpoint these areas of convective or severe weather development. Rather than large areas of potential severe weather development, the satellite soundings showed ability to locate small local maxima of moisture and instability. For example, synoptic observations may contain important information on dry line position, but only at higher resolution may we see important features of smaller scale. Rather than 100 km plus resolution, the satellite data used here provided soundings at up

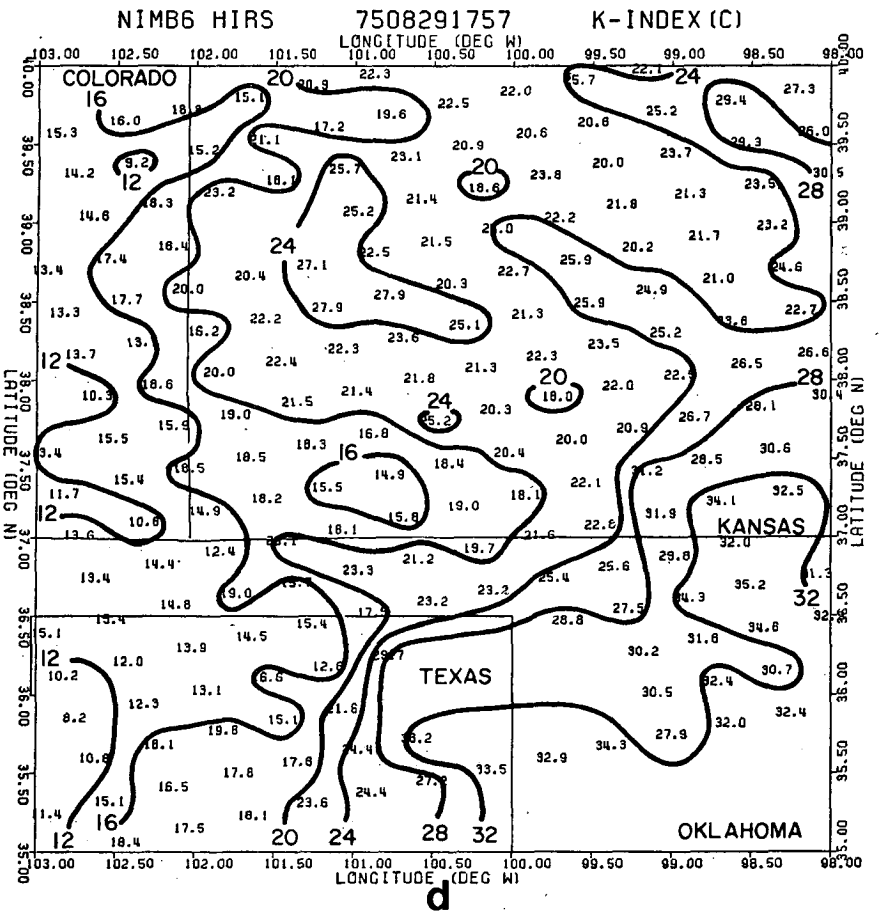

FIG. 6d. Satellite-derived K index stability analysis (°C) for 1757 GMT 29 August 1975. Contours are every 4°C.

to 30 km resolution without being oversaturated with signal noise. If clouds did not preclude the soundings there was a possibility of obtaining up to 10 times as many measurements in the same region of study. This is especially important for moisture variables since they tend to vary rapidly on small space and time scales.

These case study days also showed that there was a good capability for detecting convective development which occurred starting at least 2 h after the local noon satellite sounding time. This lead time and better resolution are special advantages of high-density soundings. Similar results using high-resolution soundings have been accomplished by Smith *et al.* (1978 and 1979) using radiances from the same HIRS instrument and showing the applicability to TIROS-N (HIRS-2) radiances.

The third analysis was not a comparison to any conventional measurements or fields of measurements. A structure function analysis gave low intrinsic noise levels for the various satellite-derived parameters. The results indicated the high quality of the mesoscale analyses. Noise levels of less than 1 K rms for temperatures, less than 1.5 K for dew point temperatures, and less than 2 mm for total precipitable water are as good as can be expected from any high-resolution sounding system. Signal-to-noise ratios also showed that the satellite-derived moisture parameters (especially surface dew point temperature) have the best information content of the parameters extracted.

These three analysis schemes, therefore, gave a definite indication of the high quality of the moisture and stability fields that can be produced by HIRS-type instruments. The mesoscale analyses also showed that the true value of satellite data will be shown in mesoscale situations where high horizontal resolution is an advantage. By using the satellite-derived mesoscale analyses along with satellite-derived winds or surface winds we could have an indication of mesoscale moisture convergence patterns. Improvements also may be possible by using other pieces of information from newer satellite instruments. To be able to use the extra channels

TABLE 4. Composite structure analysis of satellite-derived parameters for the four case study days.

Satellite-derived parameter at ~1800 GMT	rms difference at minimum separation of 33 km[a]	Standard deviation of all values in field[b]	Signal-to-noise ratio
Temperature			
surface (°C)	0.73	2.08	2.74
85 kPa (°C)	0.58	0.97	1.66
70 kPa (°C)	0.42	0.72	1.70
50 kPa (°C)	0.33	0.56	1.71
30 kPa (°C)	0.22	0.36	1.61
Brightness temperature T_B (°C)	2.76	5.17	1.85
Sensible-heat (°C)	1.35	2.71	2.00
Total PW (mm)	1.88	6.52	3.67
Dew-point temperature			
surface (°C)	1.38	4.66	3.43
85 kPa (°C)	1.23	3.12	2.63
70 kPa (°C)	1.07	2.66	2.58
Cross-total (K)	1.41	3.48	2.50
Total-total (K)	1.27	3.29	2.64
K index (°C)	2.41	6.04	2.58
Latent heat [mm (g kg^{-1})$^{-1}$]	0.092	0.166	1.80

[a] Based on approximately 400 pairs per day.
[b] Based on approximately 200 values per day.

available with HIRS-2 on TIROS-N (Schwalb, 1978), which was launched in fall 1978, will require only slight modification of the moisture-temperature retrieval scheme. An increase in the number of independent or partially independent pieces of information can hopefully further improve results. Such mesoscale analyses could, therefore, become more commonplace since the HIRS-2 system is now the operational sounding system on NOAA polar-orbiting satellites.

Acknowledgments. The authors wish to thank Mr. Harold Woolf of the Mesoscale Applications Branch of NESS at the University of Wisconsin for the HIRS transmittance software. HIRS radiances were provided by J. P. Gary, GARP DST Manager, at NASA Goddard Space Flight Center. Funding for this work was provided in part by NASA Grant NSG 5259 and by NSF Grant ATM 7918513.

REFERENCES

Chahine, M. T., 1968: Determination of the temperature profile in an atmosphere from its outgoing radiance. *J. Opt. Soc. Amer.*, **58**, 1634–1637.

——, H. H. Aumann, and F. W. Taylor, 1977: Remote sounding of cloudy atmospheres. III. Experimental verifications. *J. Atmos. Sci.*, **34**, 758–765.

Gary, J. P., 1977: AOIPS data base management systems support for GARP data sets. NASA Tech. Memo. 78-42, 36 pp.

Gandin, L. S., 1963: *Objective Analysis of Meteorological Fields*. Translated from Russian, Israel Program for Scientific Translations, Jerusalem, 242 pp. [NTIS TT-65-50007].

Hillger, D. W., and T. H. Vonder Haar, 1977: Deriving mesoscale temperature and moisture fields from satellite radiance measurements over the United States. *J. Appl. Meteor.*, **16**, 715–726.

——, and ——, 1979: An analysis of satellite infrared soundings at the mesoscale using statistical structure and correlation functions. *J. Atmos. Sci.*, **36**, 287–305.

Kelly, G. A. M., G. A. Mills and W. L. Smith, 1978: Impact of Nimbus-6 temperature soundings on Australian region forecasts. *Bull. Amer. Meteor. Soc.*, **59**, 393–405.

Lilly, D. K., (Ed.), 1975: *Open SESAME, Severe Environmental Storms and Mesoscale Experiment, Proceedings of Open Meeting*. Boulder, CO, 4–6 September 1974, 499 pp. [NTIS COM-75-11394/4GI].

——, 1977: *Project SESAME (Severe Environmental Storms and Mesoscale Experiment), Planning Documentation Volume*. NOAA/ERL, Boulder, CO, 308 pp. [NTIS PB-267 084/2GI].

Miller, R. C., 1972: Notes on analysis and severe-storm forecasting procedures of the Air Force Global Weather Central. AWS Tech. Rep. 200 [NTIS AD-744 042].

——, and R. A. Maddox, 1975: Use of the SWEAT and SPOT indices in operational severe storm forecasting. *Preprints Ninth Conf. Severe Local Storms*, Amer. Meteor. Soc., Norman, 1–6.

Project SESAME, 1976: Project Development Plan. NOAA/ERL, Boulder, CO, 60 pp.

Reitan, C. H., 1960: Distribution of precipitable water vapor over the continental United States. *Bull. Amer. Meteor. Soc.*, **41**, 79–87.

Rhea, J. O., 1966: A study of thunderstorm formation along dry lines. *J. Appl. Meteor.*, **5**, 58–63.

Schaefer, J. T., 1973: The motion of the dry line. *Preprints Eighth Conf. Severe Local Storms*, Amer. Meteor. Soc., Denver, CO, 104–107.

——, 1974: The life cycle of the dry line. *J. Appl. Meteor.*, **13**, 444–449.

Schwalb, A., 1978: The TIROS-N/NOAA A-G satellite series. NOAA Tech. Memo. NESS 95, 75 pp.

Shaw, J. H., M. T. Chahine, C. B. Farmer, L. D. Kaplin, R. A. McClatchey and P. W. Schaper, 1970: Atmospheric and surface properties from spectral radiance observations in the 4.3 micron region. *J. Atmos. Sci.*, **27**, 773–780.

Shen, W. C., and W. L. Smith, 1973: Statistical estimation of precipitable water with SIRS-B water vapor radiation measurements. *Mon. Wea. Rev.*, **101**, 24–32.

Smith, W. L., 1970: Iterative solution of the radiative transfer equation for the temperature and absorbing gas profile of an atmosphere. *Appl. Opt.*, **9**, 1993–1999.

——, and H. B. Howell, 1971: Vertical distribution of atmospheric water vapor from satellite infrared spectrometer measurements. *J. Appl. Meteor.*, **10**, 1026–1034.

——, and P. K. Rao, 1973: The determination of surface temperature from satellite "window" radiation measurements. *Temperature: Its Measurement and Control in Science and Industry*, Vol. 4, Reinhold, 2251–2257.

——, P. G. Abel, H. M. Woolf, A. W. McCulloch and B. J. Johnson, 1975: The high resolution infrared radiation sounder (HIRS) experiment. *The Nimbus 6 User's Guide*, 37–58 [NTIS N76-31256/OGI].

——, C. M. Hayden, H. M. Woolf, H. B. Howell and F. W. Nagle, 1978: Interactive processing of TIROS-N sounding data. *Preprints, Conf. Weather Forecasting and Aviation Meteorology*, Silver Spring, Amer. Meteor. Soc. 390–395.

——, ——, ——, —— and ——, 1979: Satellite sounding applications to mesoscale meteorology. *Remote Sounding of the Atmosphere from Space*, COSPAR, Innsbruck, 33–47.

——, H. M. Woolf, P. G. Abel, C. M. Hayden, M. Chalfant and N. Grody, 1974: Nimbus 5 sounder data processing system, Part 1. NOAA Tech. Memo. NESS 57, 99 pp. [NTIS COM-74-11436/4GI].

Storm Data, 1975: NOAA, Environmental Data Service, National Climatic Center, **16**, No. 8.

Tracton, M. S., and R. D. McPherson, 1977: On the impact of radiometric sounding data upon operational numerical weather prediction at NMC. *Bull. Amer. Meteor. Soc.*, **58**, 1201–1209.

Wark, D. Q., J. H. Lienesch and M. P. Weinreb, 1974: Satellite observations of atmospheric water vapor. *Appl. Opt.*, **13**, 507–511.